



Structure-activity relationship study: Mechanism of cyto-genotoxicity of Nitropyrazole-derived high energy density materials family

Laetitia Guyot, Florian Simon, Jessica Garcia, Floriane Vanhalle, Gaelle Vilchez, Claire Bardel, Brigitte Manship, Alain Puisieux, Christelle Machon, Guy Jacob, et al.

► To cite this version:

Laetitia Guyot, Florian Simon, Jessica Garcia, Floriane Vanhalle, Gaelle Vilchez, et al.. Structure-activity relationship study: Mechanism of cyto-genotoxicity of Nitropyrazole-derived high energy density materials family. Toxicology and Applied Pharmacology, 2019, 381, pp.114712 -. 10.1016/j.taap.2019.114712 . hal-03487645

HAL Id: hal-03487645

<https://hal.science/hal-03487645>

Submitted on 20 Dec 2021

HAL is a multi-disciplinary open access archive for the deposit and dissemination of scientific research documents, whether they are published or not. The documents may come from teaching and research institutions in France or abroad, or from public or private research centers.

L'archive ouverte pluridisciplinaire **HAL**, est destinée au dépôt et à la diffusion de documents scientifiques de niveau recherche, publiés ou non, émanant des établissements d'enseignement et de recherche français ou étrangers, des laboratoires publics ou privés.



Distributed under a Creative Commons Attribution - NonCommercial 4.0 International License

Structure-activity relationship study: mechanism of cytogenotoxicity of Nitropyrazole-derived high energy density materials family

Laetitia Guyot^{1,2} Florian Simon¹ Jessica Garcia¹ Floriane Vanhalle¹ Gaelle Vilchez¹ Claire Bardel¹ Brigitte Manship² Alain Puisieux^{2,3} Christelle Machon¹ Guy Jacob^{4,5} Jérôme Guitton^{1,3,*} Léa Payen^{1,2,3}

¹ Hospices Civils de Lyon, Centre Hospitalier Lyon-Sud, Laboratoire de biochimie-toxicologie, France.

² UMR INSERM U1052/CNRS 5286, Centre de Recherche en Cancérologie de Lyon, Centre Léon Bérard, France.

³ Université Lyon 1, ISPBL, Faculté de pharmacie, Laboratoire de Toxicologie, France.

⁴ Université Lyon 1, Faculté des sciences et technologies, UMR CNRS 5278 Hydrazines et Composés Energetiques Polyazotés, France.

⁵ ArianeGroup Centre de Recherche du Bouchet, France

* To whom correspondence should be addressed: Pr. J. Guitton, Université Lyon 1, ISPBL, Faculté de pharmacie, Laboratoire de Toxicologie, 8 avenue Rockefeller, 69373, Lyon, France.

E-mail: jerome.guitton@univ-lyon1.fr

Abstract

Stringent toxicological tests have to be performed prior to the industrial development of alternative chemicals particularly high energy dense materials (HEDMs) such as explosives. The properties (e.g., power, stability) of these compounds are constantly being improved, the current axis of research being the nitration of nitrogen heterocycles leading to HEDMs such as nitropyrazole-derived molecules. However, except for 3,4,5-trinitropyrazole (3,4,5-TNP), which was shown to be highly toxic in mice, the toxicological impact of these HEDMs has so far not been investigated. Furthermore, as industrials are strongly advised to develop alternative safety testing assays to *in vivo* experiments, we herein focused on determining the cytotoxic and genotoxic effects of seven Nitropyrazole-derived HEDMs on three rodent cell lines (mouse embryonic BALB/3T3 clone A31 cells, Chinese hamster ovary cells CHO-K1 and mouse lymphoma L5178Y TK +/- clone (3.7.2C) cells), two human fibroblast lines (CRC05, PFS04062) and on the human hepatic HepaRG model (both in proliferative and differentiated cells). A stronger cytotoxic effect was observed for 1,3-dinitropyrazole (1, 3-DNP) and 3,4,5-TNP in all cell lines, though differentiated HepaRG cells clearly displayed fewer likely due to the metabolism and elimination of these molecules by their functional biotransformation pathways. At the mechanistic level, the sub-chronic cytotoxic and genotoxic effects were linked to ROS/RNS production (experimental assays), HA2.X and to transcriptomic data highlighting the increase in DNA repair mechanisms.

Keywords

Nitropyrazole-derived; HEDMs; RNAseq; Genotoxicity

Highlights

- * A difference in cytotoxicity (until 200 fold) is observed between the nitropyrazoles
- * The impact on the cell cycle depends on the compounds
- * Oxidative stress pathways may be involved in the cellular cytotoxicity
- * Targeted metabolomics approach shown few modifications in endogenous metabolites

50 Introduction

51 Chemical explosives are highly reactive compounds that contain both their own oxygen (reaction initiator) and fuel
52 (explosive compound) within the same molecule. Several parameters are important to the development of chemical
53 explosives for military and civilian (e.g., building industry) applications, including a positive oxygen balance (i.e., a better
54 detonator), a high enthalpy of formation (i.e., a better transfer of energy during the production of new molecules), a low
55 sensitivity (offers better stability), a high stability (thermal and chemical) and a low level of toxicity. The initial inclusion
56 of nitro functional groups (-NO₂) to well-known liquid combustibles prior to World War I (WWI) gave rise to highly
57 explosive molecules such as trinitrophenol or trinitrotoluene (TNT), while the consecutive addition of this functional group
58 to the aromatic ring of such energetic molecules generated even more powerful compounds like 1,3,5-trinitro-1,3,5-
59 triazinane (RDX) or 1,3,5,7-tetranitro-1,3,5,7-tetrazocane (HMX), used during WWII. However, owing to their instability,
60 industrials introduced hydrogen-bound amino groups to nitro-based explosives to reduce their sensitivity, as exemplified
61 in nitrotriazolone (NTO), 1,3,5-triamino-2,4,6-trinitrobenzene (TATB), and 1,1-diamino-2,2-dinitroethylene (FOX7). This
62 unfortunately affected their energetic performance, and the current axis of research into improving the balance between
63 energy and stability/sensitivity in high energy density materials (HEDMs) (Dalinger, 2010), is the nitration (addition of
64 energetic -NO₂ groups) of nitrogen heterocycles, such as in the formation of nitropyrazole-derived molecules.
65 More and more studies are investigating the environmental toxicity of HEDMs. Nevertheless, little is known about the
66 human toxicology and USEPA organization has recommended restrictions for lifetime contact through drinking water
67 (Chatterjee *et al.*, 2017). For example to limit human exposition, laboratories are developing new transgenic western
68 wheatgrass that degrades the explosive RDX and detoxifies TNT especially on live-fire training ranges, threatens
69 environmental and human health (Zhang *et al.*, 2019). Recently, very interestingly, mixture effects of the insensitive
70 munitions formulations IMX-101 (mixture of 2,4-dinitroanisole [DNAN], 3-nitro-1,2,4-triazol-5-one [NTO], and
71 nitroguanidine [NQ]) and IMX-104 (DNAN, NTO, and RDX) were evaluated in subchronic and chronic water-only assays
72 in *Hyalella azteca* assessing impacts on survival, growth and reproduction. Longer exposure duration to IMX-101, IMX-
73 104, and DNAN resulted in higher sensitivity for lethality and decreased reproduction function (Lotufo *et al.*, 2018).
74 Recently, to decipher toxicogenomic responses for the individual constituents of IMX-101, transcriptomic analysis were
75 conducted. It was found that transcriptional regulations and functional responses characteristic of: oxidative stress,
76 impaired energy metabolism, tissue damage and inflammatory responses in DNAN exposures; impaired steroid
77 biosynthesis and developmental cell-signaling in NQ exposures; and altered mitogen-activated protein kinase signaling in
78 NTO exposures (Gust *et al.*, 2018). Finally, for a molecular characterization of the RDX induced neurotoxicity, a
79 transcriptomic analysis was conducted in RDX exposed rats. They observed an induction of miRNAs expression levels by

RDX. This could reduce the expression levels of POLE4, C5ORF13, SULF1 and ROCK2 genes. RDX regulated immune and inflammation response miRNAs and genes could contribute to RDX- induced neurotoxicity and other toxicities as well as animal defending reaction response to RDX exposure (Deng *et al.*, 2014). Taken altogether, new methodologies enable researchers to decipher the toxicological molecular mechanisms of these explosive molecules.

For the purpose of our study, these include the previously studied 3,4,5-trinitropyrazole (3,4,5-TNP) by our own group (Guyot *et al.* 2018), and its precursors or derivatives: 1-nitropyrazole (1-NP), 3-nitropyrazole (3-NP), 1,3-dinitropyrazole (1,3-DNP), 3,5-dinitropyrazole (3,5-DNP), 4-nitropyrazole (4-NP), and 1-methyl 4-nitropyrazole (1-Met-4-NP). Nevertheless, excluding our own *in vivo* toxicity and pharmacokinetic evaluation of 3,4,5-TNP (Guyot *et al.* 2018), few toxicological data are available for this family of pyrazole derivatives.

Here, based both on classical OECD Testing of Chemicals Guidelines, and on previously developed human cell line models, we evaluated (i) the *in vitro* toxicological impact and (ii) mechanisms of toxicity using a transcriptomic methodology of these nitropyrazole-derived HEDMs. Indeed, a high level of cytotoxicity and genotoxicity may be a go/no go decision in the development of a new industrial molecule, and consequently the toxic risk for humans has to be evaluated following strict methods (OECD - Guidelines for the Testing of Chemicals, Section 4). In this field, various functional assays and various animal models are used including murine embryonic BALB/3T3 clone A31 cells, Chinese hamster ovary cells CHO-K1 and mouse lymphoma L5178Y TK +/- clone (3.7.2C) cells.

Furthermore, owing to the most common route of entry (inhalation/skin contact) and most common toxic side effects (hepatotoxicity; owing to its role in the biotransformation of xenobiotics) for explosive molecule developers and civilians alike, the molecules were tested in two human fibroblast cell lines and in a human hepatic cell line, namely HepaRG. These hepatic cells are the first model of human cells able to differentiate *in vitro* into mature hepatocyte-like cells, while conserving major biotransformation functions including CYP3A4 metabolism, phase 2 enzymes, transporters and regulatory transcriptional factors (Aninat *et al.* 2006; Anthérieu *et al.* 2012; Le Vee *et al.* 2013). This cell line is successfully used in toxicological studies using toxigenomics and metabolomics methodology in differentiated state or spheroid state (Van den Eede *et al.*, 2015; Bell *et al.*, 2017; Moedas *et al.*, 2017; Limonciel *et al.*, 2018; Mesnage *et al.*, 2018; Ramaiahgari *et al.*, 2019). In this work, we identified 1,3-DNP and 3,4,5-TNP as the most cytotoxic molecules, and demonstrated that toxicological and cellular effects can be globally screened using the presented transcriptomic approaches, which enabled us to gain in objectivity with regards to the toxicological impact of exposure to xenobiotics (e.g., cellular pathway dysregulations).

Materials and methods

Reagents and chemicals

Nitropyrazole-derived HEDMs were synthesized at the ArianeGroup research center (Hervé, 2007). The route involves several steps of N-Nitration and transposition of NO₂ ending by a mixed acids nitration on the carbon atom in the 4 position. These molecules were obtained either in pure water (3,4,5-TNP at 1M), in dimethyl sulfoxide (DMSO; 1,3-DNP at 100 mM and 3-NP at 1 M) or into acetonitrile (ACN; 1-NP, 4-NP and 1-Met-4-NP at 1M and 3,5-DNP at 770 mM; Table 1); the initial choice of solvent depending on their physicochemical properties. Nitropyrazole-derived HEDMs were stored at 4°C in the dark under a slight nitrogen stream. Doxorubicin, DMSO, ammonium sulfate, and ACN (HPLC grade) were purchased from Sigma-Aldrich (Saint-Quentin Fallavier, France). Acetic acid (Ultra-pure, > 99.5%) and ammonia (30%) were purchased from Carlo Erba reagents (Milano, Italy). Milli-Q deionized water was used throughout the study. Drug-free normal plasma was provided by the regional blood bank (EFS Rhône-Alpes, France).

Tissue culture

L5178Y TK +/- clone (3.7.2C), CHO-K1 (ATCC® CCL61™), and BALB/3T3 clone A31 (ATCC® CCL163™) cells were purchased from the ATCC biological resources center (<https://www.lgcstandards-atcc.org>). The tissue culture conditions strictly followed guidelines provided by the ATCC. HepaRG cells were purchased from Biopredic International (Rennes, France) and cultured according to their guidelines. Two primary human normal fibroblast cell lines, PSF04062 and CRC05, were cultured in DMEM (Dulbecco's Modified Eagle Medium, Life Technologies (#31966047)) supplemented with 10% FCS, 100 units/ml penicillin, 100 µg/ml streptomycin, and 2 mM glutamine.

Cytotoxicity and cell proliferation assays

To evaluate the cytotoxicity of nitropyrazole-derived molecules, two methods were applied, namely, the MTT assay to assess cell viability and the xCELLigence technique for a dynamic monitoring of cell viability and proliferation. Briefly, for the MTT assay, cells were seeded onto 96-well culture plates at a density of 1,000-8,000 cells/well (according to the rate of proliferation of the studied cell line). The cells were exposed to Nitropyrazole-derived HEDMs (at a final concentration ranging from 0.0016 mM to 10 mM) for 72 h, and cell viability/growth/proliferation was then assessed by applying MTT (3-(4,5-dimethylthiazol-2-yl)-2,5-diphenyltetrazolium bromide) to the cells. Formazan production was measured spectrophotometrically at OD = 550 nm (MultiSkanAscent, ThermoFisher Scientific™ #51118407). The following formula was used to determine the IC₅₀ (%) (inhibitory concentration) = ((OD of the sample - OD of the control)/(OD of the control))x100. For each condition four technical and at least three independent biological measurements were obtained.

140 The xCELLigence system (ACEA Biosciences, San Diego, CA, USA) was used following the manufacturer's protocol. In
141 this system, 2000-5000 cells are grown in special chambers where they adhere to gold-coated microelectrodes that measure
142 the relative change in electrode impedance, expressed as a cell index (CI), a unit less parameter, as a function of time. This
143 measurement provides dynamic information on the number of cells attached/proliferating. Cells were then either treated
144 with various concentrations of Nitropyrazole-derived HEDMs or similar amounts of vehicle. The CI value of each group
145 was monitored for 5 days. Each condition was duplicated, and at least three independent experiments were carried out.

146

147 **RNA expression and quantitative real time PCR (RT-PCR) assays**

148 Total RNA was extracted and purified using the RNeasy Mini Kit (Qiagen # 74106). Amounts of RNA isolated from
149 samples can vary due to the developmental stage, species, and growth conditions of the original sample. Furthermore, the
150 RNeasy procedure enriches RNA species >200 nt and excludes 5S rRNA, tRNAs, or other low molecular weight RNAs.
151 RNA was isolated on the silica membrane in trusted RNeasy spin columns, with binding capacities of 100 µg of RNA,
152 according to the supplier's recommendations (Qiagen). The expression levels of various genes were quantified by PCR
153 using the BIORAD CFX96 Touch™ (BIORAD, #1855195). The reverse transcription was carried out using Maxima First
154 Strand cDNA Synthesis Kit (ThermoFisher #K-1642).

155

156 **mRNA library preparation for next generation sequencing (NGS)**

157 For the preparation of the NGS RNA library, RNA concentration was measured using the GE NanoView
158 Spectrophotometer (Biochrom US, Holliston, MA, US). The quality of RNA samples was analyzed using the RNA 6000
159 Pico Kit running on the 2100 BioAnalyzer (Agilent Santa Clara, California, US). Total RNA samples were diluted to 20
160 ng/µL in a final volume of 50 µL for a total input of 1 µg. Only the RNA pools with a RIN score higher than 9 were used
161 in the NGS library preparation prior to sequencing. Firstly, mRNAs were isolated using the NEBNext Poly(A) mRNA
162 Magnetic Isolation Module from 1 µg of total RNA. The isolation procedure is based on the selection of mRNA using
163 oligo dT beads directed against polyA tails of intact mRNA. Secondly, the NGS libraries were created from mRNA isolated
164 using the NEBNext Ultra II Directional RNA Library Prep Kit for Illumina (NewEngland BioLabs, Ipswich,
165 Massachusetts). The sequencing reads were obtained after demultiplexing the raw sequencing data using bcl2fastq
166 v2.19.1.403 (Version v2.15.0 for NextSeq™ 500 and HiSeq® X Systems, Illumina). After validating the quality controls
167 of each sample using the FastQC v0.11.5 software (<https://www.bioinformatics.babraham.ac.uk/projects/fastqc/>). The
168 alignment files were generated with STAR v2.5.2b (University of Birmingham) in the 2-pass mode. We used the hg19
169 human genome as reference. This mode is known to improve the detection of more reads mapping novel splice junctions.

170 Once the final sorted alignment file was obtained, the count of reads was done with the GFOLD V1.1.4 (option – count;
171 <https://bitbucket.org/feeldead/gfold/>) and the GENCODE annotation file of the human genome
172 ([gencode.v19.annotation.gtf](https://www.gencodegenes.org/); <https://www.gencodegenes.org/>) (Feng *et al.*, 2012; Dobin *et al.*, 2013). The differential
173 expression of genes was then calculated with GFOLD-diff bioinformatics pipeline. For this final step, GFOLD pipeline
174 values were the mean of three independent samples The heatmap representation was carried out using the Xlstat software
175 (<https://www.xlstat.com/fr/solutions/biomed>)

176 **Flow cytometry**

177 The quantity of H₂O₂ was estimated using an indicator of ROS in cells (CM-H₂DCFDA; reference #C6827), and RNS
178 derivatives using a nitric oxide indicator (DAF-FM; reference #D23841) according to the manufacturer's instructions
179 (Thermo Fisher Scientific). Whole-cell fluorescence intensity was quantified by flow cytometry using a BD FACSCalibur
180 (BD Biosciences, Grenoble, France) with 10,000 events recorded. The final data were analyzed using the FlowLogic
181 Software (Miltenyi Biotec GmbH, Bergisch Gladbach, Germany). Each condition was duplicated, and at least three
182 independent experiments were carried out.

183

184 **H2A.X phosphorylation on Serine 139**

185 Differentiated HepaRG cells were treated with nitropyrazole-derived HEDMs. After trypsinization, cells were resuspended
186 in 500 µL of 1X Assay Buffer (included in the kit, Catalog No. MCH200101) per one million cells. Equal parts of Fixation
187 Buffer were added to cell suspensions. Cells were then permeabilized by adding 1 mL ice-cold 1X Permeabilization Buffer
188 per one million cells and incubated on ice for 5 min. After washing, cells were resuspended in 90 µL of 1X Assay Buffer.
189 10 µL of the antibody working cocktail solution (5 µL of antiphospho-histone H2A.X (Ser139), Alexa Fluor® 555 and 5
190 µL of anti-histone H2A.X, PECy5 conjugated) were added to each experimental condition and incubated for 30 min at
191 room temperature (RT) in the dark. After washing, the fluorescence of nuclear foci was visualized via the Muse™ Cell
192 Analyzer using the onscreen instructions.

193

194 **Quantification of LDH, glucose, and lactate**

195 Using the ARCHITECT C16000 Clinical Chemistry Analyzer (Abbott Laboratories, Chicago, Illinois, US), and their
196 validated CE-IVD kits, lactate dehydrogenase (LDH), glucose (GLU) and lactate contents were quantified (Guyot *et al.*,
197 2018). Each condition was duplicated, and at least three independent experiments were carried out. Glucose consumption
198 is defined as the difference between the initial glucose concentration and the glucose remaining at the end of the experiment.
199 Similarly, the secretion of lactate and LDH are calculated by the difference between their initial and final concentrations.

200

201 **Cell cycle exploration**

202 HepaRG cells in a proliferative phase were treated with Nitropyrazole-derived HEDMs for 24 h. We then added 30 μ M of
203 5-bromo-2'-deoxyuridine (BrdU) for 1 h. After trypsinization, cells were washed with PBS 1X, and fixed using 70%
204 ethanol. Again, cells were washed with PBS 1X and treated with 2 mol/L HCl for 20 min at RT. Cells were washed with
205 0.5% BSA 0.5% Tween in PBS (PBT), incubated with an anti-BrdU conjugated with FITC (BD Biosciences; dilution 1/10
206 in PBT) for 30 min at RT in the dark, and then washed with PBT. After resuspension of cells into 100 μ L of PBS, cells
207 were incubated for 30 min in the dark at RT with RNase at a final concentration of 100 μ g/mL (Sigma-Aldrich St. Louis,
208 MO US). 300 μ L of PBS were then added and the cells were incubated with 20 μ g/mL propidium iodide (PI). Whole-cell
209 fluorescence intensity was measured by FACS using a BD LSR Fortessa™ flow cytometer (BD Biosciences, Grenoble,
210 France) with 10,000 events recorded. The final data were analyzed using the FlowLogic Software (Miltenyi Biotec GmbH,
211 Bergisch Gladbach, Germany). Each condition was replicated, and at least three independent experiments were carried out.

212

213 **Apoptosis assay (Annexin V labeling)**

214 Differentiated HepaRG cells were treated with Nitropyrazole-derived HEDMs for 24 h and 72 h. Cells were trypsinized
215 and diluted to 100,000 cells/mL in a buffer (PBS 1x + SVF 1%). 100 μ L of the Muse™ Annexin V & Dead Cell Reagent
216 Kit; MCH100105) was added to 100 μ L of each condition. Following 20 min of staining at RT, data were acquired by flow
217 cytometry with the Muse™ Cell Analyzer using the onscreen instructions.

218

219 **Targeted metabolomics**

220 At the end of the exposition of differentiated HepaRG cells, the culture medium was removed and cells were washed three
221 times with cold PBS 1X. For samples destined to nucleotide determination, cold methanol/water (v/v: 70/30) was added,
222 while in samples used for the determination of other metabolites, cold methanol/water (v/v: 70/30) and 3% formic acid
223 were added. Samples were stored at -80°C until analysis. Sample preparation was performed as follows: labeled internal
224 standards (4 for nucleotides and 27 for other metabolites) were added to cellular extracts which were vigorously vortexed
225 and centrifuged for 10 min at 13,000 g. Supernatants were evaporated to dryness under nitrogen at 37 °C. The residues
226 were resuspended in 200 μ L and 100 μ L of mobile phase before injection, for metabolites and nucleotides, respectively.
227 Targeted metabolomic analyzes were performed by liquid chromatography coupled with a tandem high resolution mass
228 spectrometer (Q-Exactive Plus Orbitrap, Thermo Scientific, Bremen, Germany). The high resolution mass spectrometer
229 was operated alternatively in positive and negative ionization mode. Full scan and dd-MS² (data dependent MS/MS) modes

230 were used with a resolution set at 70,000 and 17,500, respectively. Metabolites were identified using retention time,
231 accurate mass of parent compound, isotopic pattern and daughter ions.

232

233 **Statistics**

234 All statistical analyses were performed using the GraphPad InStat software 7.00 (GraphPad Software; La Jolla, CA USA).
235 The non-parametric test for significance was performed when the number of samples (N) was below 30. Non-parametric
236 tests for non- normalized data or for n<30 and a two-way ANOVA were performed for normalized data. A 2-sided P-value
237 of < 0.05 was considered statistically significant.

238 **RESULTS**

239

240 **Effect of nitropyrazole-related molecules on proliferation and viability of rodent and human cell models**

241 HEDM-induced cytotoxicity, measured either *via* MTT assays or using the xCELLigence system for the nitropyrazole-
242 derived HEDMs listed in Table 1, was determined in murine L5178Y TK +/- clone (3.7.2C) and BALB/3T3 clone A31
243 cells and in Chinese hamster CHO-K1 cells (Table 2; Supplementary Figure S1a-c), as well as in human PFS04062
244 fibroblasts (Table 2; Supplementary Figure S1d) and human hepatocytes-like HepaRG cells (Table 3; Supplementary
245 Figure S1e-f). Unfortunately, L5178Y TK +/- clone (3.7.2C) BALB/3T3 clone A31 cells could not be tested using the
246 xCELLigence analysis since they did not adhere to the chamber, while the CRC05 human fibroblasts were not tested. For
247 some xCELLigence experiments, the highest dose of the HEDMs was tested or the determined MTT CI50 concentration.
248 The xCELLigence allowed us to confirm the MTT findings. However, data (presented in Table 2) revealed that, except for
249 1-nitropyrazole (1-NP), both techniques led to very similar results. Indeed, the half maximum inhibitory concentration or
250 IC₅₀ of the nitropyrazole-derived HEDMs obtained *via* the MTT assay when applied to the xCELLigence system blocked
251 cell proliferation in a dose-dependent manner and in the same range as the MTT assay, except for 1-NP which appeared to
252 have no effect on cells in the latter test. This could be due to the different parameters measured (mitochondrial activity for
253 the MTT assay *vs* cellular confluence for the xCELLigence) or to the assay conditions (different surfaces of adhesion...).

254 The first noteworthy result is the clear cytotoxic effect of 1,3-dinitropyrazole (1,3-DNP) and 3,4,5-trinitropyrazole (3,4,5-
255 TNP) on all three rodent cell models compared to the other four nitropyrazole-derived HEDMs. This is illustrated by the
256 clear shift in cell viability curves (Supplementary Figure S1a-c) after the incubation of cells with 1,3-DNP and 3,4,5-TNP
257 concentrations 50-200 fold lower (0.002-0.04 mM) than 1-NP, 3-NP, 3,5-DNP, 4-NP and 1-methyl 4-nitropyrazole (1-
258 Met-4-NP) (0.4- > 10 mM; Table 2). Though the effects of 3,5-DNP and 1-Met-4-NP were difficult to differentiate between
259 these cell lines, (i) BALB/3T3 clone A31 cells were more resistant to 1-NP, 3-NP and 4-NP than L5178Y TK +/- clone

260 (3.7.2C) and CHO-K1 cells, and (ii) 1-NP affected L5178Y TK +/- clone (3.7.2C) cells more than CHO-K1 cells, while
261 this was the opposite for 3-NP and was indistinctive for 4-NP (Table 2). The cytotoxic effects of HEDM molecules were
262 independently confirmed in CHO-K1 using the xCELLigence assay.

263 In human adult PFS04062 and CRC05 fibroblasts, the IC₅₀ were in the same range for 3-NP, 3,5-DNP, 4-NP and 1-Met-
264 4-NP (except in CRC05 in which the level of cytotoxicity was not be determined). Overall, a 10-fold greater IC₅₀ was
265 measured in human fibroblasts than in animal fibroblasts, suggesting a stronger resistance of human dermic fibroblasts to
266 the nitropyrazole-derived HEDMs. Furthermore, in the case of PFS04062 the effect of these molecules was more marked
267 when looking at the proliferating cell index (CI) of the xCELLigence method (Table 2). Once again, the most cytotoxic
268 molecule was 1,3-DNP, followed by 3,4,5-TNP (as evidenced in the Supplementary Figure S1d). This was also true for
269 human HepaRG hepatocytes, both in a proliferative and differentiated stage (Table 3; Supplementary Figure S1e-f).
270 However, these two stages displayed several interesting differences as 1,3-DNP and 1-NP had a 10-fold and 3,5-NP had
271 an ~4-fold greater effect on proliferative cells, while 3,4,5-TNP had a similar IC₅₀ in both stages (Table 3).

272 Finally, the impact of Nitropyrazole-derived HEDMs on the cell cycle of proliferative HepaRG cells was studied for 24 h,
273 and a cytostatic effect of 1,3-DNP, 3,4,5-TNP and 3,5-DNP was found. These molecules blocked the cell cycle of HepaRG
274 cells in the S and G2M phases, and decreased the proportion of HepaRG cells in the G1 phase. In contrast, exposure to 1-
275 NP led to a decrease in cells in the S phase, indicating an impairment in DNA replication. The other molecules did not
276 modify the proportion of cells in the different phases (Table 3). Altogether, our findings led us to propose the resulting
277 cytotoxicity ranking in all of the cell lines tested above: 1,3-DNP>>> 3,4,5-TNP>> 3,5-DNP \cong 1-NP >3-NP = 4-NP = 1-
278 Met-4-NP.

279

280 **Effects of Nitropyrazole-derived HEDMs on physiological pathways in differentiated HepaRG cells**

281 Owing to the vital role played by hepatocytes in the biotransformation of xenobiotics and to the frequent accumulation of
282 toxic molecules/derivatives in these cells, the remainder of our study focuses on the physiopathological effects of
283 Nitropyrazole-derived HEDMs on differentiated HepaRG cells. Consistently, we attempted to mimic a sub-chronic
284 exposure to non-deadly concentrations of these HEDMs and verified their impact on cellular functions (major cell signaling
285 pathways).

286 We initially evaluated the effect doses of nitropyrazole-derivatives over 24 h on the rate of cell death, by measuring LDH
287 release into the medium of differentiated HepaRG cells. Indeed, LDH release is a validated early biomarker for the
288 induction of cytolysis and can be measured via flow cytometry. Under our experimental conditions no detectable cytolysis
289 was observed in differentiated Hepa-RG cells (Supplementary Table S1). Under these conditions, we studied the biological

effect of the highest doses of HEDMs could experimentally be used. To confirm that this was not due to a lack of uptake of the nitropyrazole-derived HEDMs, the intracellular accumulation of Nitropyrazole-derived HEDMs was carried out by liquid chromatography coupled with tandem high resolution mass spectrometry (LC-HRMS). Four nitropyrazole-derived HEDMs were quantified, clearly showing an uptake of these compounds into cells (Supplementary Table S2). Unfortunately, we were unable to quantify 1-NP, 1,3-DNP and 1-Met-4-NP using LC-HRMS, since they do not contain any ionizable groups (Bader *et al.*, 1998; Coombs and Schillack, 1998). However, since the other nitropyrazole-derived HEDMs were taken up (Supplementary Table S2), this strongly suggests that these compounds should also penetrate into cells and reassured us as to our interpretations of our regulatory findings even if no biological effects were observed. As shown above, 1,3-DNP, 3,4,5-TNP and 3,5-DNP blocked the cell cycle at the S and G2M stages in proliferative cells. Though differentiated HepaRG cells reached confluence after 24 h incubation with the three nitropyrazole-derived HEDMs, these were able to modify the level of expression of transcripts of genes involved in cell cycle regulation (Supplementary Figure S2). The strongest transcript up-regulations (represented in red on the heat-map in Supplementary Figure 2S) were observed with 1,3-DNP. In parallel, the expression levels of genes involved in death pathways (necrosis, senescence, autophagy and apoptosis) were analyzed and little modifications in autophagy, necrosis and senescence were observed (Table 4). When examining the apoptosis signaling pathway, we subdivided the actors according to their pro- and anti-apoptotic functions (Supplementary Figure S3), and found some variations at the transcriptomic level both for pro- and anti-apoptotic factors (Supplementary Figure S3). Based on Annexin V labeling (see Materials and Methods for details) we studied the number of cells undergoing early and late stage apoptosis after 24 h and 72 h incubation with nitropyrazole-derived HEDMs but found no differences with controls (vehicles) under our experimental conditions (Table 5), suggesting that the variations in gene expression levels were not sufficient to increase cell death rates.

311

312 **Identification of the initial events leading to modifications in physiological processes**

313 In parallel, we also evaluated the impact of these HEDMs on physiopathological pathways including known genotoxic
314 pathways responsible for cancer initiation (first step in the carcinogenesis process), oxidative stresses due to reactive
315 nitrogen species (RNS) and reactive oxygen species (ROS) production since they are largely involved in toxicological
316 pathways. We also studied metabolite biosynthesis, such as the amino acids, nucleic acid derivatives and organic acid
317 derivatives, since they modify the proliferation rate and energy cellular biosynthesis. The genotoxicity of nitropyrazole-
318 derived HEDMs was indirectly studied in human differentiated HepaRG cells based on two complementary approaches,
319 namely by assessing (i) the regulation of genes involved in DNA repair pathways and (ii) the number of nuclear foci upon

phosphorylation of the Serine P139 residue on the H2AX protein (a marker of activation of the double-strand break DNA repair system) using the Muse™ H2A.X. Clearly, an up-regulation in the expression levels of DNA repair genes was observed after 24 h exposure to non-deadly concentrations of 1,3-DNP, 3,4,5-TNP and 3,5-DNP, while only a slight down regulation was noted for the other molecules (Fig. 1a). Furthermore, though no increase in the number of γ -H2AX foci was quantified after 2 h exposure to nitropyrazole-derived HEDMs, at 24 h an increase was observed for 3-NP, 1,3-DNP, 3,4,5-TNP and 3,5-DNP (Fig. 1b). This effect was stronger for 3,4,5-TNP.

To study the putative drivers of genotoxicity, both ROS (H_2O_2) and RNS derivatives were measured in differentiated HepaRG cells exposed to nitropyrazole-derived HEDMs. The expression levels of genes implicated in oxidative and radical pathways were inversely regulated by the cytotoxic nitropyrazole-derived HEDMs and the weakly cytotoxic molecules (Fig. 2a). We observed an increase in expression levels of genes encoding proteins involved in the protection against oxidative stresses, including GSTA1 and SOD, after incubation with 1-NP, 3-NP, 4-NP, 1-Met-4-NP, while these transcripts were down-regulated by the cytotoxic nitropyrazole-derived HEDMs (1,3-NP, 3,4,5-TNP and 3,5-DNP). These findings indicate that oxidative stress pathways may be involved in the cellular cytotoxicity caused by these nitropyrazole-derived HEDMs (Fig. 2a). ROS production was then quantified after 90 min using CM- H_2 DCFDA probes (Fig. 2b), the 1 mM was the highest tested concentration of HEDMs, we could test under our experimental condition (we limited the percentage of DMSO exposure to 0.5%). Both 1,3-DNP and 3,4,5-TNP significantly increased cellular ROS levels, while the other nitropyrazole-derived HEDMs displayed no significant modifications under our experimental conditions. Using DAF-FM probes, intracellular RNS levels were also quantified after 60 min following the same assay conditions as for ROS measurement. Interestingly, 1,3-DNP, 3,4,5-TNP and 3,5-DNP were able to significantly increase RNS production in cells, while 1-NP, 4-NP, and 1-Met-4-NP did not induce any change for RNS production at 1 mM and 3NP induced a decrease for RNS production at a final assay concentration of 1 mM (Fig. 2c).

341

342 **Metabolomic findings**

343 Having observed an increase in ROS production in differentiated HepaRG cells treated with 1,3-DNP and 3,4,5-TNP, as
344 well as an increase in RNS production, we assumed that these molecules may modify the production of energy by cells
345 (ATP, amino acids, acid organic). Lactate secretion and glucose consumption by differentiated HepaRG cells exposed to
346 varying concentrations of nitropyrazole-derived HEDMs were quantified after 6 h, 24 h and 48 h. A significant increase in
347 lactate secretion into the medium was only observed for 1-NP, 4-NP, 3,5-DNP and 3-NP after 24 h and 48 h, while glucose
348 levels strongly decreased after 48 h exposure (Supplementary Table S3). Additionally, some transcripts of genes involved
349 in energy producing pathways were up-regulated following exposure to 3-NP, 1-NP and 1-Met-4-NP nitropyrazole-derived

HEDMs, whereas the other nitropyrazole-derived HEDMs slightly down-regulated these metabolic pathway actors (Fig. 3a). To complete this transcriptomic study, pools of approximately 40 endogenous physiological compounds were measured (expressed in fold-change) after 36 h of exposure to these nitropyrazole molecules. At this time it was also performed the transcriptional and post-transcriptional effects of the HEDMs on metabolomics functions of the cells. Very few modifications in endogenous pools were observed (Supplementary Table S4). Creatine, cysteine, N-acetylspermidine pools were increased under 1,3-DNP and 3,5-DNP treatments. Alanine pool was increased under 3,5-DNP and 3-NP treatments. 3,4,5-TNP treatment decreased 5-hydroxyindolacetic acid and putrescine pools (Supplementary Table S4 and Fig. 3b).

DISCUSSION

To validate the use of novel, more powerful and stable HEDMs in military or civilian applications, their toxic side effects have to be tested following rigorous OECD guidelines. Here, we initially tested the cytotoxicity of seven nitropyrazole-derived molecules; 1-nitropyrazole (1-NP), 3-nitropyrazole (3-NP), 1,3-dinitropyrazole (1,3-DNP), 3,5-dinitropyrazole (3,5-DNP), 3,4,5-trinitropyrazole (3,4,5-TNP), 4-nitropyrazole (4-NP), and 1-methyl 4-nitropyrazole (1-Met-4-NP), using three animal cell lines listed in the database of the European Centre for the Validation of Alternative Methods (ECVAM) and OCDE organization (OECD - Guidance Document on Good In Vitro Method Practices (GIVIMP)). These databases enable researchers to perform alternative *in vitro* toxicity tests on previously validated models, thus improving their acceptance by regulators and facilitating the toxicological assessment/comparison of molecules. Based on their IC₅₀, we determined the cytotoxic ranking for all of the nitropyrazole-derived HEDMs in the three rodent cell lines (BALB/3T3 clone A31, CHO-K1 and L5178Y TK +/- clone (3.7.2C)), exposing 1,3-DNP and 3,4,5-TNP as the most cytotoxic. Interestingly, this ranking was identical for these cell lines, as well as for human fibroblasts (CRC05, PFS04062) and hepatocytes (HepaRG). HepaRG cells were then more extensively studied, as they strongly express biotransformation enzymes (Aninat *et al.*, 2006; Antherieu *et al.*, 2012) and are most likely to accumulate xenobiotics (Le Vee *et al.*, 2013). The cytotoxicity ranking for these cells resembled that observed with other cell lines with 1,3-DNP, 3,5-DNP and 3,4,5-TNP having the strongest effects. To ascertain whether this effect was due to an increase in cell death or to a cytostatic effect, we studied their impact on the cell cycle and clearly showed that 1,3-DNP, 3,5-DNP and 3,4,5-TNP blocked cells in the S and G2M stage, while the proportion of cells in S phase strongly decreased with 1-NP. This clearly indicated that these molecules block the proliferation pathway. Interestingly, after differentiation their level of cytotoxicity largely decreased suggesting that the biotransformation capacities of HepaRG cells metabolized and eliminated these molecules.

379 Differentiated HepaRG cells is currently used and validated by the ECVAM to explore the hepatotoxic effects of drugs
380 (Aninat et al. 2006; Anthérieu et al. 2011, 2012; Sharanek et al. 2014; Truisi et al. 2015; Pomponio et al. 2015). The
381 biotransformation capability of differentiated HepaRG cells had a particular interest here since previous works on
382 nitrofurantoin or nitroimidazole indicated that nitro-group determines hepatic cytotoxicity through reactive intermediates
383 such as nitroso and hydroxylamine derivatives (Li *et al.*, 2019; Nepali *et al.*, 2019). Moreover, TNT is a known genotoxic
384 (Ahlborg et al. 1988), we were initially interested in investigating the genotoxicity of the nitropyrazole-derived HEDMs,
385 and this is usually *via* the Ames and the micronuclei tests. The former is based on bacterial cells, and the latter principally
386 murine cell lines. The genotoxicity of some nitro imidazole derivatives, such as benznidazole (2-nitro-N-(phenylmethyl)-
387 1H-imidazole-1-acetamide), have already been described in the Ames test (Ferreira and Ferreira, 1986). This genotoxicity
388 effect has been directly linked to nitroreductases expressed in salmonella. Interestingly, it has been argued that the lower
389 capacity of mammalian cells to perform nitroreduction decreases the genotoxic risk of 5-nitromegazol (Buschini *et al.*,
390 2007). Then, we proposed to evaluate genotoxicity effects using mammalian cells. Owing to the difference in cytotoxicity
391 between species found in our first experiments, we evaluated this parameter in the human differentiated HepaRG model
392 by (i) quantifying the phosphorylation of Ser139 on H2A.X, a hallmark of DNA repair machinery activation, and (ii)
393 through transcriptomic analysis to highlight DNA repair pathway genes regulated by these HEDMs. Both techniques
394 revealed that 1,3-DNP and 3,4,5-TNP activated DNA reparation mechanisms. This effect was attended as 5-nitroimidazol
395 compounds increase DNA damages through the so-called futile cycle, i.e. one electron reduction of the drug leads to the
396 production of nitro radical anions which in the presence of oxygen are oxidized and may generate reactive oxygen species
397 (ROS) (Re *et al.*, 1997; Nepali *et al.*, 2019). The nitro radical anion and nitroso derivatives, or esterified hydroxylamine
398 (e.g., sulfate derivatives) are associated with the mutagenicity (Bolt *et al.*, 2006). Superoxide anions, hydrogen peroxide,
399 and hydroxyl radicals formed during the redox cycling of the nitro radical anion may also lead to carcinogenicity (Nepali
400 *et al.*, 2019). Then, to identify in our present study the early driver of this genotoxicity, we quantified the production of
401 radical stresses (RNS and ROS) in HepaRG cells and concomitantly evaluated the expression of genes involved in these
402 pathways. Our findings strongly suggest the role of radical stress in nitropyrazole-derived genotoxicity, corroborating
403 previous studies on TNT but also on 5-nitroimidazole (Bolt *et al.*, 2006; Nepali *et al.*, 2019). This hypothesis was supported
404 by several reports in which the generation of oxidative stress by diazinon, was decreased by antioxidant molecules co-
405 exposition in various cellular models (Ahmadi *et al.*, 2015; Ahmadi and Shadboorestan, 2016; Karamian *et al.*, 2016).
406 Since oxidative stress plays a crucial role in the pathophysiology of tumors, in our work support, the use of appropriated
407 measures for the prevention of occupational hazards of 1,3-DNP and 3,4,5-TNP compounds. Since the other HEDMs

408 molecules contain nitro radical anion, actions under the precautionary principle should be implemented (Nepali *et al.*,
409 2019)

410 Similarly, to TNT studies, we explore the molecular toxicological mechanisms of the HEDMs. Indeed, one of the possible
411 mechanisms of toxicity of TNT and some of its metabolic intermediates is the generation of reactive oxygen species that
412 cause injury to the lens leading to the formation of cataracts and lipid peroxidation in the live. This is supported by the fact
413 that at high levels in the air, workers involved in the production of TNT experience anemia and liver function abnormalities,
414 as well skin irritation and cataracts after long-term exposure (Letzel *et al.*, 2003). Since, industries have been strongly
415 recommended to limit the use of *in vivo* models, it is of vital importance that *in vitro* strategies are developed and that data
416 can be transposed to *in vivo* situations, such as through the use of transcriptomics (Deng *et al.*, 2010). Indeed, these authors
417 revealed that gene regulatory networks obtained from an *in vitro* system could predict *in vivo* functions and mechanisms.
418 In their study, 341 common transcripts were differentially expressed *in vitro* and *in vivo* in response to TNT, and they
419 reported that inhibiting PTTG1 and its targeted cell cycle-related genes in the liver could be a key mechanism for TNT-
420 induced liver toxicity. These authors also proposed that the development of mathematical simulation tools could improve
421 *in vitro* data interpretation (Deng *et al.*, 2010). In the present study, we also clearly established the regulation of genes
422 modulating common pathways *in vitro*, and provided a complete overview of the principal toxic effects and physiological
423 impacts of nitropyrazole-derived HEDMs in HepaRG cells. Furthermore, most of the changes in gene expression observed
424 after nitropyrazole exposure were accompanied by modifications in functional biomarkers, including RNS and ROS pools,
425 H2A.X serine 139 phosphorylation, and activation of apoptosis. This approach thus seems to be of great interest, and merits
426 further investigation.

427 In agreement with our transcriptomic approach, researchers have utilized a novel high-throughput transcriptomics (HTT)
428 platform to apply the interpretive power of concentration-response modeling with exposures to reference compounds in
429 both differentiated and non-differentiated human HepaRG cell cultures. They explored transcriptomic characteristics
430 distinguishing liver injury compounds, and assess impacts of differentiation state of HepaRG cells on baseline and
431 compound-induced responses (e.g., metabolically-activated), and identify and resolve reference biological-response
432 pathways through benchmark concentration modeling. Similarly to our data, impacts of cellular differentiation state
433 (proliferated vs. differentiated) were revealed on baseline drug metabolizing enzyme expression, hepatic receptor signaling,
434 and responsiveness to metabolically-activated toxicants (e.g., cyclophosphamide, benzo(a)pyrene, and aflatoxin B1)
435 (Ramaiahgari *et al.*, 2019). Taken together, these findings confirmed the predictive value of toxicological level obtained
436 using *in vitro* liver models avoiding the use of *in vivo* experiments.

Since non-alcoholic Fatty Liver Disease (NAFLD) is a frequently encountered Drug-Induced Liver Injury (DILI). Although this stage of the disease is reversible, it can lead to irreversible damage provoked by non-alcoholic steatohepatitis (NASH), fibrosis and cirrhosis. Therefore, the assessment of NAFLD is a paramount objective in toxicological screenings of new industrial compounds. Recently, it has been reported a metabolomic fingerprint of NAFLD induced in HepaRG cells at four dosing schemes by a reference toxicant, sodium valproate (NaVPA), using liquid-liquid extraction followed by liquid chromatography and accurate mass-mass spectrometry (LC-AM/MS). Increased levels of S-adenosylmethionine and mono-acetylspermidine in combination with only a moderate increase in triglycerides was observed first and in second time, spermidines, creatine, and acetylcholine were modified, signing a steatotic progression. In our report, only creatine, cysteine, N-acetylspermidine pools were increased under 1,3-DNP and 3,5-DNP treatments were modified, suggesting a possible risk of steatosis activation (Cuykx *et al.*, 2018).

In conclusion, the present study demonstrated the cytotoxicity of seven nitropyrazole-derived HEDMs in differentiated HepaRG cells and particularly the genotoxic effect of 1,3-DNP and 3,4,5-TNP that increase DNA double-strand breaks, likely *via* the production of ROS/RNS molecules. This study shows that the position of nitro-group on the pyrazole nucleus have an influence on the cytotoxicity level as previously demonstrated for nitro-imidazole derivatives (Boechat *et al.*, 2015).

Compliance with ethical standards

Not applicable

Conflict of interest

Authors declare no conflict of interest

Funding

This work was supported by institutional grants from ArianeGroup. LG was recipient of fellowships from ArianeGroup.

References

- Ahmadi, A., Shadboorestan, A., 2016. Oxidative stress and cancer; the role of hesperidin, a citrus natural bioflavonoid, as a cancer chemoprotective agent. *Nutr Cancer* **68**, 29-39.
- Ahmadi, A., Shadboorestan, A., Nabavi, S.F., Setzer, W.N., Nabavi, S.M., 2015. The Role of Hesperidin in Cell Signal Transduction Pathway for the Prevention or Treatment of Cancer. *Curr Med Chem* **22**, 3462-3471.
- Aninat, C., Piton, A., Glaise, D., Le Charpentier, T., Langouet, S., Morel, F., Guguen-Guillouzo, C., Guillouzo, A., 2006. Expression of cytochromes P450, conjugating enzymes and nuclear receptors in human hepatoma HepaRG cells. *Drug Metab Dispos* **34**, 75-83.
- Antherieu, S., Chesne, C., Li, R., Guguen-Guillouzo, C., Guillouzo, A., 2012. Optimization of the HepaRG cell model for drug metabolism and toxicity studies. *Toxicol In Vitro* **26**, 1278-1285.
- Bader, M., Goen, T., Muller, J., Angerer, J., 1998. Analysis of nitroaromatic compounds in urine by gas chromatography-mass spectrometry for the biological monitoring of explosives. *J Chromatogr B Biomed Sci Appl* **710**, 91-99.
- Bell, C.C., Lauschke, V.M., Vorrink, S.U., Palmgren, H., Duffin, R., Andersson, T.B., Ingelman-Sundberg, M., 2017. Transcriptional, Functional, and Mechanistic Comparisons of Stem Cell-Derived Hepatocytes, HepaRG Cells, and Three-Dimensional Human Hepatocyte Spheroids as Predictive In Vitro Systems for Drug-Induced Liver Injury. *Drug Metab Dispos* **45**, 419-429.
- Boechat, N., Carvalho, A.S., Salomao, K., Castro, S.L., Araujo-Lima, C.F., Mello, F.V., Felzenszwalb, I., Aiub, C.A., Conde, T.R., Zamith, H.P., Skupin, R., Haufe, G., 2015. Studies of genotoxicity and mutagenicity of nitroimidazoles: demystifying this critical relationship with the nitro group. *Mem Inst Oswaldo Cruz* **110**, 492-499.
- Bolt, H.M., Degen, G.H., Dorn, S.B., Plottner, S., Harth, V., 2006. Genotoxicity and potential carcinogenicity of 2,4,6-TNT trinitrotoluene: structural and toxicological considerations. *Rev Environ Health* **21**, 217-228.
- Buschini, A., Giordani, F., de Albuquerque, C.N., Pellacani, C., Pelosi, G., Rossi, C., Zucchi, T.M., Poli, P., 2007. Trypanocidal nitroimidazole derivatives: relationships among chemical structure and genotoxic activity. *Biochem Pharmacol* **73**, 1537-1547.
- Chatterjee, S., Deb, U., Datta, S., Walther, C., Gupta, D.K., 2017. Common explosives (TNT, RDX, HMX) and their fate in the environment: Emphasizing bioremediation. *Chemosphere* **184**, 438-451.
- Coombs, M., Schillack, V., 1998. Determination of trinitrotoluene and metabolites in urine by means of gas-chromatography with mass detection. *Int Arch Occup Environ Health* **71 Suppl**, S22-25.
- Cuykx, M., Claes, L., Rodrigues, R.M., Vanhaecke, T., Covaci, A., 2018. Metabolomics profiling of steatosis progression in HepaRG((R)) cells using sodium valproate. *Toxicol Lett* **286**, 22-30.
- Dalinger, I.L., Vatsadze, I.A., Shkineva, T.K., 2010. The specific reactivity of 3,4,5-trinitro-1H-pyrazole. *Mendeleev Commun.* **20**, 253-254.
- Deng, Y., Ai, J., Guan, X., Wang, Z., Yan, B., Zhang, D., Liu, C., Wilbanks, M.S., Escalon, B.L., Meyers, S.A., Yang, M.Q., Perkins, E.J., 2014. MicroRNA and messenger RNA profiling reveals new biomarkers and mechanisms for RDX induced neurotoxicity. *BMC Genomics* **15 Suppl 11**, S1.
- Deng, Y., Johnson, D.R., Guan, X., Ang, C.Y., Ai, J., Perkins, E.J., 2010. In vitro gene regulatory networks predict in vivo function of liver. *BMC Syst Biol* **4**, 153.
- Dobin, A., Davis, C.A., Schlesinger, F., Drenkow, J., Zaleski, C., Jha, S., Batut, P., Chaisson, M., Gingeras, T.R., 2013. STAR: ultrafast universal RNA-seq aligner. *Bioinformatics* **29**, 15-21.
- Feng, J., Meyer, C.A., Wang, Q., Liu, J.S., Shirley Liu, X., Zhang, Y., 2012. GFOLD: a generalized fold change for ranking differentially expressed genes from RNA-seq data. *Bioinformatics* **28**, 2782-2788.

- Ferreira, R.C., Ferreira, L.C., 1986. Mutagenicity of CL 64855, a potent anti-*Trypanosoma cruzi* drug. *Mutat Res* **171**, 11-15.
- Gust, K.A., Lotufo, G.R., Stanley, J.K., Wilbanks, M.S., Chappell, P., Barker, N.D., 2018. Transcriptomics provides mechanistic indicators of mixture toxicology for IMX-101 and IMX-104 formulations in fathead minnows (*Pimephales promelas*). *Aquat Toxicol* **199**, 138-151.
- Guyot, L., Honorat, M., Jacob, G., Bardel, C., Tod, M., Puisieux, A., Guitton, J., Payen, L., 2018. Toxicokinetics and tolerance of a high energy material 3,4,5-trinitropyrazole (TNP) in mice. *Toxicol Appl Pharmacol* **355**, 103-111.
- Karamian, A., Shokrzadeh, M., Ahmadi, A., 2016. The potential chemoprotective effects of melatonin against genotoxicity induced by diazinon in human peripheral blood lymphocytes. *Toxicol Ind Health* **32**, 360-366.
- Le Vee, M., Noel, G., Jouan, E., Stieger, B., Fardel, O., 2013. Polarized expression of drug transporters in differentiated human hepatoma HepaRG cells. *Toxicol In Vitro* **27**, 1979-1986.
- Letzel, S., Goen, T., Bader, M., Angerer, J., Kraus, T., 2003. Exposure to nitroaromatic explosives and health effects during disposal of military waste. *Occup Environ Med* **60**, 483-488.
- Li, H., Zhang, Z., Yang, X., Mao, X., Wang, Y., Wang, J., Peng, Y., Zheng, J., 2019. Electron Deficiency of Nitro Group Determines Hepatic Cytotoxicity of Nitrofurantoin. *Chem Res Toxicol* **32**, 681-690.
- Limonciel, A., Ates, G., Carta, G., Wilmes, A., Watzele, M., Shepard, P.J., VanSteenhouse, H.C., Seligmann, B., Yeakley, J.M., van de Water, B., Vinken, M., Jennings, P., 2018. Comparison of base-line and chemical-induced transcriptomic responses in HepaRG and RPTEC/TERT1 cells using TempO-Seq. *Arch Toxicol* **92**, 2517-2531.
- Lotufo, G.R., Stanley, J.K., Chappell, P., Melby, N.L., Wilbanks, M.S., Gust, K.A., 2018. Subchronic, chronic, lethal and sublethal toxicity of insensitive munitions mixture formulations relative to individual constituents in *Hyalella azteca*. *Chemosphere* **210**, 795-804.
- Mesnage, R., Biserni, M., Balu, S., Frainay, C., Poupin, N., Jourdan, F., Wozniak, E., Xenakis, T., Mein, C.A., Antoniou, M.N., 2018. Integrated transcriptomics and metabolomics reveal signatures of lipid metabolism dysregulation in HepaRG liver cells exposed to PCB 126. *Arch Toxicol* **92**, 2533-2547.
- Moedas, M.F., Adam, A.A.A., Farelo, M.A., L, I.J., Chamuleau, R., Hoekstra, R., Wanders, R.J.A., Silva, M.F.B., 2017. Advances in methods for characterization of hepatic urea cycle enzymatic activity in HepaRG cells using UPLC-MS/MS. *Anal Biochem* **535**, 47-55.
- Nepali, K., Lee, H.Y., Liou, J.P., 2019. Nitro-Group-Containing Drugs. *J Med Chem* **62**, 2851-2893.
- Ramaiahgari, S.C., Auerbach, S.S., Saddler, T.O., Rice, J.R., Dunlap, P.E., Sipes, N.S., DeVito, M.J., Shah, R.R., Bushel, P.R., Merrick, B.A., Paules, R.S., Ferguson, S.S., 2019. The Power of Resolution: Contextualized Understanding of Biological Responses to Liver Injury Chemicals using High-throughput Transcriptomics and Benchmark Concentration Modeling. *Toxicol Sci.*
- Re, J.L., De Meo, M.P., Laget, M., Guiraud, H., Castegnaro, M., Vanelle, P., Dumenil, G., 1997. Evaluation of the genotoxic activity of metronidazole and dimetridazole in human lymphocytes by the comet assay. *Mutat Res* **375**, 147-155.
- Van den Eede, N., Cuykx, M., Rodrigues, R.M., Laukens, K., Neels, H., Covaci, A., Vanhaecke, T., 2015. Metabolomics analysis of the toxicity pathways of triphenyl phosphate in HepaRG cells and comparison to oxidative stress mechanisms caused by acetaminophen. *Toxicol In Vitro* **29**, 2045-2054.
- Zhang, L., Rylott, E.L., Bruce, N.C., Strand, S.E., 2019. Genetic modification of western wheatgrass (*Pascopyrum smithii*) for the phytoremediation of RDX and TNT. *Planta* **249**, 1007-1015.
- OECD - Guidelines for the Testing of Chemicals, Section 4. https://www.oecd-ilibrary.org/environment/oecd-guidelines-for-the-testing-of-chemicals-section-4-health-effects_20745788. (accessed 15 October 2018).

563
564
565
566
567

OECD - Guidance Document on Good In Vitro Method Practices (GIVIMP).
<http://www.oecd.org/fr/env/ess/guidance-document-on-good-in-vitro-method-practices-givimp-9789264304796-en.htm>. (accessed 5 April 2019).

Figures and Tables

Fig. 1 Effect of nitropyrazole-derived HEDMs on DNA repair mechanisms of differentiated HepaRG cells. **a** Gene analysis of DNA damage pathways by RNASeq following the incubation of differentiated HepaRG cells with 1 mM 1-nitropyrazole (1-NP), 1 mM 3-nitropyrazole (3-NP), 0.05 mM 1,3-dinitropyrazole (1,3-DNP), 1 mM 3,5-dinitropyrazole (3,5-DNP), 0.250 mM 3,4,5-trinitropyrazole (3,4,5-TNP), 1 mM 4-nitropyrazole (4-NP) or 1 mM 1-methyl 4-nitropyrazole (1-Met-4-NP) for 24 h. Results are expressed in log2 fold change and assigned a blue (decrease in expression) or red (increase in expression) color. The heat map was obtained with the XLSstat software, and the data shown represent three independent experiments. **b** Overlay of flow cytometry results for H2AX and γ H2AX foci quantification for HepaRG cells treated as in (a). Each nitropyrazole is compared cells treated with its relevant vehicle. 20 μ M doxorubicin was used as a positive control. Flow cytometry plots are representative of 2 independent experiments. *MeOH* methanol, *ACN* acetonitrile, *DMSO* dimethyl sulfoxide

Fig. 2 Evaluation of the effect of nitropyrazole-derived HEDMs 1 mM 1-nitropyrazole (1-NP), 1 mM 3-nitropyrazole (3-NP), 0.05 mM 1,3-dinitropyrazole (1,3-DNP), 1 mM 3,5-dinitropyrazole (3,5-DNP), 0.250 mM 3,4,5-trinitropyrazole (3,4,5-TNP), 1 mM 4-nitropyrazole (4-NP) or 1 mM 1-methyl 4-nitropyrazole (1-Met-4-NP) on cellular stress in differentiated HepaRG cells. **a** Transcriptomic analysis by RNASeq of genes implicated in the DNA damage pathway. Differentiated HepaRG were treated with nitropyrazole-derived HEDMs for 24 h. Results are expressed in log2 fold change and data were assigned a blue (decrease in expression) or red (increase in expression) color. The heat map was obtained with the XLSstat software, and the data represent three independent experiments. **b** Reactive oxygen species (ROS) were measured using the CM-H₂DCFDA probe in differentiated HepaRG cells incubated for 30 min with a positive control (1 mM H₂O₂), and either 90 min with equivalent amounts of vehicles (negative control), or nitropyrazole-derived HEDMs as in (a). Total ROS production was quantified by flow cytometry as the mean fluorescence intensity of cells. Data are expressed as mean \pm S.E.M. of at least two independent experiments. **c** Quantification of NO reactive derivatives (RNS) was performed through the measurement of intracellular DAF-FM accumulation by flow cytometry in differentiated HepaRG cells treated for 60 min with nitropyrazole-derived HEDMs as in (a). Data are expressed as the percentage increase (mean \pm S.E.M.) in mean fluorescence intensity of total NO reactive derivatives (RNS) for at least two independent experiments. Control cells were incubated with equivalent amounts of vehicles. Statistical analysis (Mann-Whitney) was conducted using GraphPad, NS not significant; * $P < 0.05$; ** $P < 0.01$ *ACN* acetonitrile, *DMSO* dimethyl sulfoxide

Fig. 3 Effect of Nitropyrazole-derived HEDMs 1 mM 1-nitropyrazole (1-NP), 1 mM 3-nitropyrazole (3-NP), 0.05 mM 1,3-dinitropyrazole (1,3-DNP), 1 mM 3,5-dinitropyrazole (3,5-DNP), 0.250 mM 3,4,5-trinitropyrazole (3,4,5-TNP), 1 mM 4-nitropyrazole (4-NP) or 1 mM 1-methyl 4-nitropyrazole (1-Met-4-NP) on metabolomics of differentiated HepaRG cells, assessed by **(a)** gene analysis (RNASeq) after 24 h incubation. Results are represented in log2 fold change and assigned a blue (decrease in expression) or red (increase in expression) color. The heat map was obtained with the XLSstat software, and the data represent three independent experiments. **b** Targeted metabolites were also quantified in HepaRG cells treated for 36 h as in **(a)** by LC-HRMS. Data are expressed as mean \pm S.E.M. of at least three independent experiments.

Tables:

Table 1 Overview of the different nitropyrazole-derived HEDMs used throughout this study, as well as their corresponding concentration, chemical structure and molecular weight. *ACN* acetonitrile, *DMSO* dimethyl sulfoxide

Table 2 Cellular cytotoxicity of various concentrations of nitropyrazole-derived HEDMs measured using either an MTT assay (cell viability) or the xCELLigence technology (cell proliferation). **a** The first three columns indicate the half maximum inhibitory concentration (IC_{50}) obtained following MTT assays in the rodent CHO-K1, BALB/3T3 clone (A31), L5178T TK+/- (clone 3.7.2C) cells, after 72 h exposure to the indicated nitropyrazole-derived HEDMs (their respective vehicles are indicated in brackets). Data are expressed as mean \pm S.D (N > 3 independent experiments). The last column presents xCELLigence results obtained in the only rodent cell line that grew in the specific xCELLigence chambers, namely the CHO-K1 cells. This shows the percentage of viable cells (compared to the vehicle condition) after incubation with nitropyrazole-derived molecules, the initial concentrations of which were obtained through the MTT assays. Statistical analysis (One-way ANOVA) was conducted using GraphPad, NS not significant; * $P < 0.05$; ** $P < 0.01$. **b** The first two columns present MTT assays in human PSF04062 and CRC05 fibroblast cells after 72 h exposure to the indicated nitropyrazole molecules. Data are expressed as mean \pm S.D (N > 2 independent experiments), ND not determined. The last column shows results obtained with the xCELLigence technology in human PSF04062 cells. Data are expressed as percentage of viable cells compared to vehicle (untreated) conditions. Statistical analysis (One-way ANOVA) was conducted using GraphPad, NS not significant; * $P < 0.05$; ** $P < 0.01$.

ACN acetonitrile, *DMSO* dimethyl sulfoxide, *NP* nitropyrazole, *DNP* dinitropyrazole, *TNP* trinitropyrazole, *M* methyl

627 **Table 3** Cytotoxic effects of various concentrations of nitropyrazole-derived HEDMs on proliferative and differentiated
628 HepaRG cells. The first part of the table indicates the half maximum inhibitory concentration (IC₅₀) of the molecules
629 incubated with proliferative or differentiated HepaRG cells for 72 h, obtained by MTT assays. All data represent the mean
630 \pm S.D. of at least three separate experiments. The second part of the table reports the effect of these molecules on the cell
631 cycle of proliferative HepaRG cells, measured via a flow cytometry analysis of BrdU incorporation into cells over 24 h.
632 Data are expressed as mean \pm S.D. of at least two independent experiments. Statistical significance (One-way ANOVA)
633 was obtained using the GraphPad software. *NS* not significant; * $P < 0.05$; ** $P < 0.01$; *** $P < 0.001$; **** $P < 0.0001$.

634 *ACN* acetonitrile, *DMSO* dimethyl sulfoxide, *NP* nitropyrazole, *DNP* dinitropyrazole, *TNP* trinitropyrazole, *M* methyl
635
636

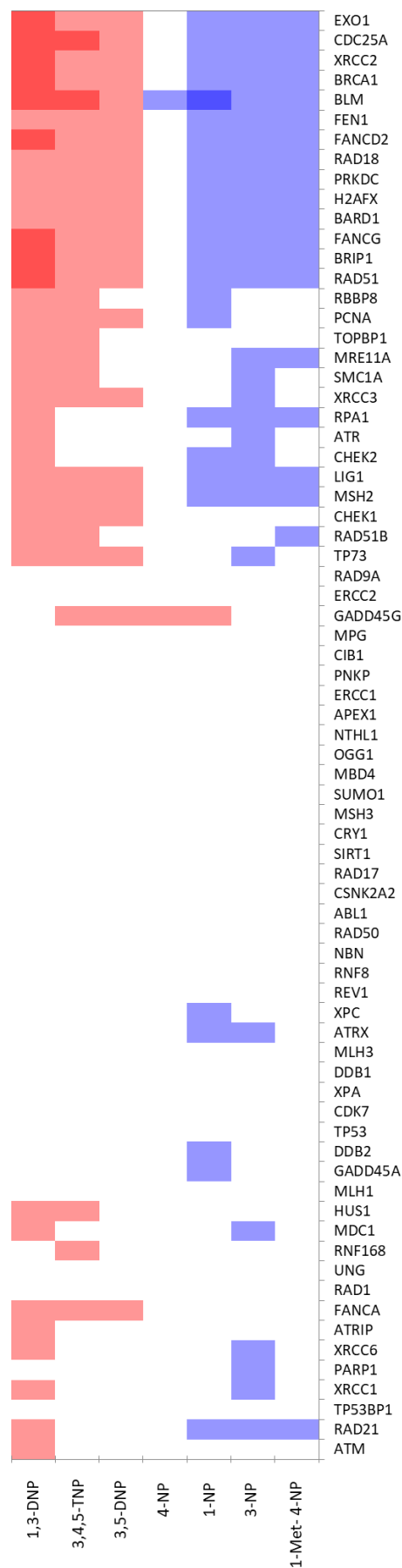
637 **Table 4** Variation in the expression of transcripts involved in cell death mechanisms in differentiated HepaRG cells treated
638 for 24 h with Nitropyrazole-derived HEDMs at the following concentrations 1 mM 1-nitropyrazole (1-NP), 1 mM 3-
639 nitropyrazole (3-NP), 0.05 mM 1,3-dinitropyrazole (1,3-DNP), 1 mM 3,5-dinitropyrazole (3,5-DNP), 0.250 mM 3,4,5-
640 trinitropyrazole (3,4,5-TNP), 1 mM 4-nitropyrazole (4-NP) or 1 mM 1-methyl 4-nitropyrazole (1-Met-4-NP). This table
641 presents the list of genes studied for the necrosis, the autophagy and the senescence pathways by RNAseq. Only genes
642 with at least 50% of variation, either an increase (\uparrow) or a decrease (\downarrow) are represented for each molecule. The log 2 fold
643 changes were calculated using the vehicles as controls. The data represent three independent experiments.

644
645 **Table 5** Proportion of apoptotic cells (early and late stage apoptosis) following the incubation of differentiated HepaRG
646 cells with nitropyrazole-derived HEDMs for 24 h and 72 h. The final assay concentrations were 1 mM 1-nitropyrazole (1-
647 NP), 1 mM 3-nitropyrazole (3-NP), 0.05 mM 1,3-dinitropyrazole (1,3-DNP), 1 mM 3,5-dinitropyrazole (3,5-DNP), 0.250
648 mM 3,4,5-trinitropyrazole (3,4,5-TNP), 1 mM 4-nitropyrazole (4-NP) or 1 mM 1-methyl 4-nitropyrazole (1-Met-4-NP).
649 These results were obtained with the Muse® Annexin V and Dead Cell Assay Kit. Data are expressed as mean \pm S.E.M. of
650 at least two independent experiments. Statistical analysis (Two-way ANOVA) was conducted using the GraphPad
651 software. *NS* not significant, * $P < 0.05$.

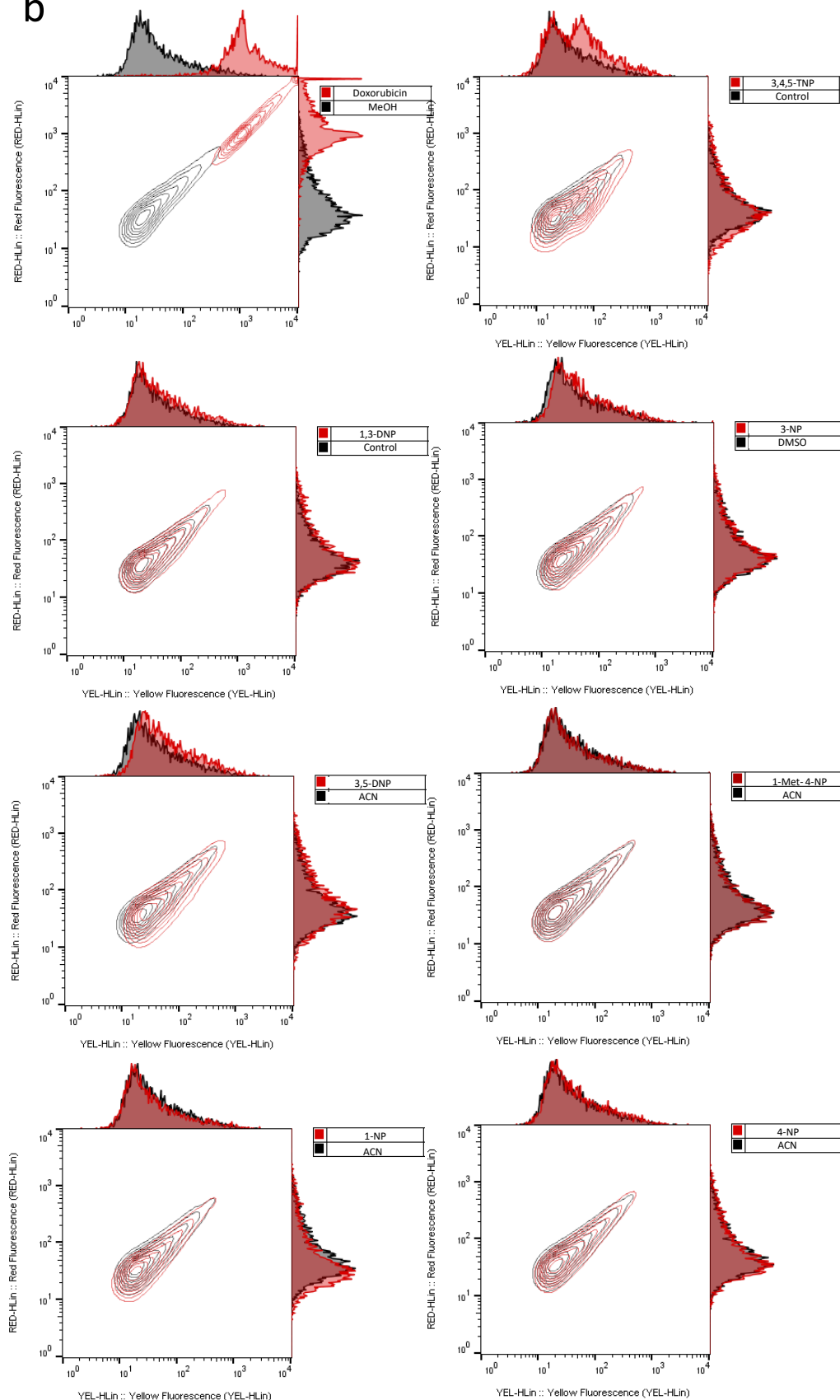
652

653

a



b



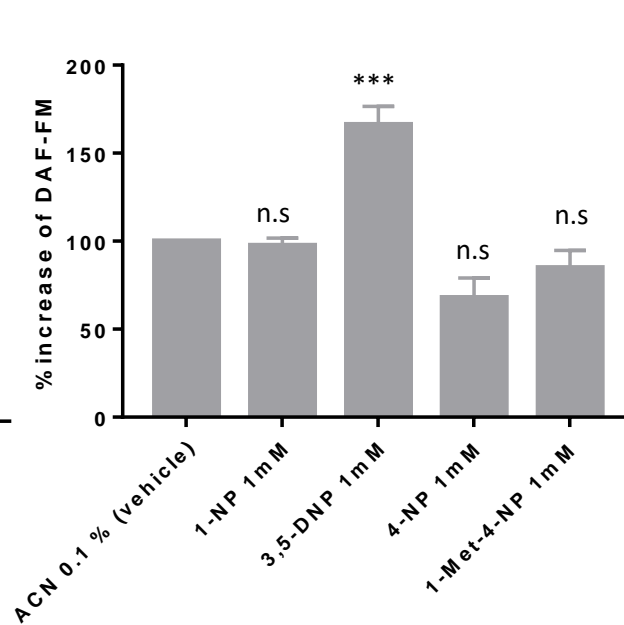
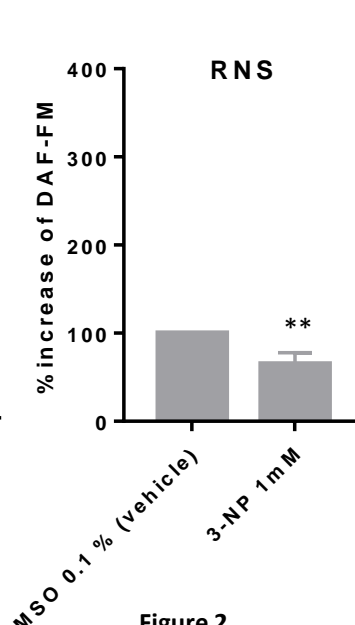
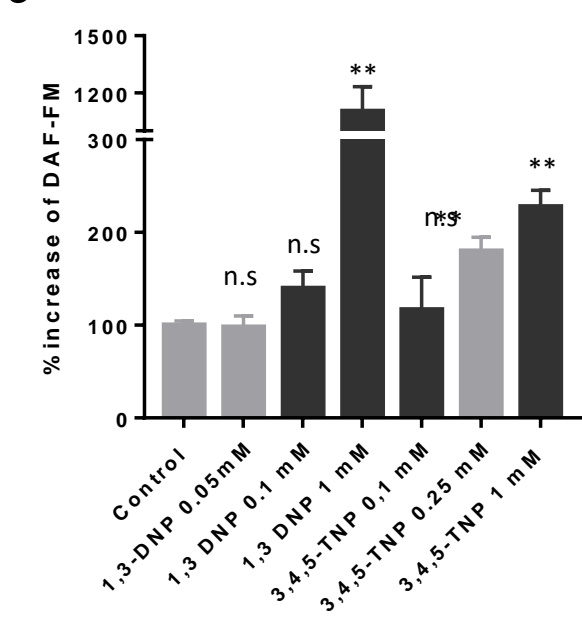
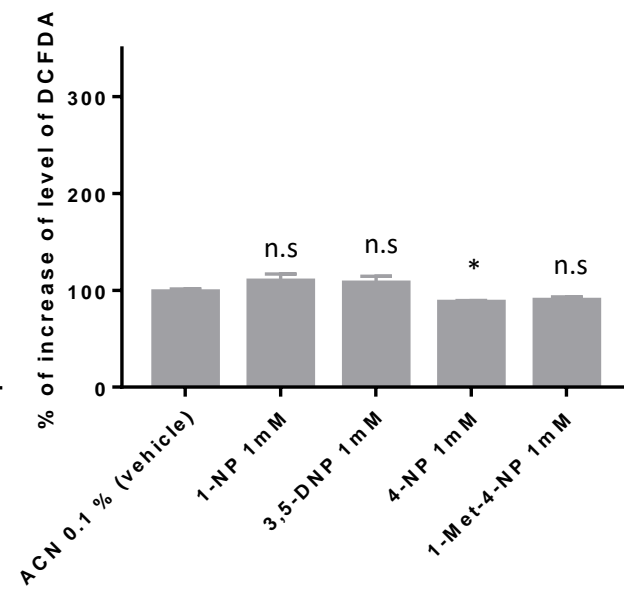
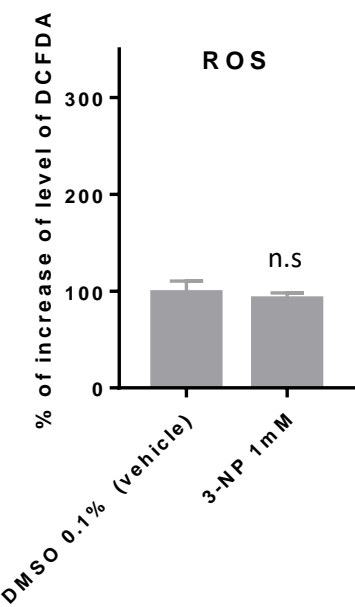
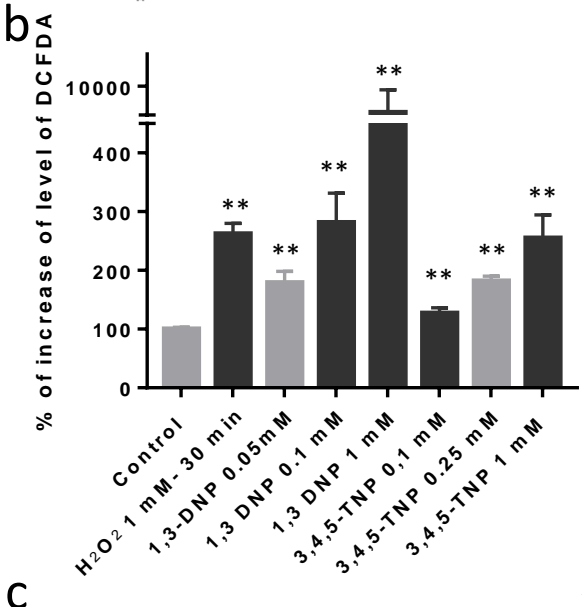
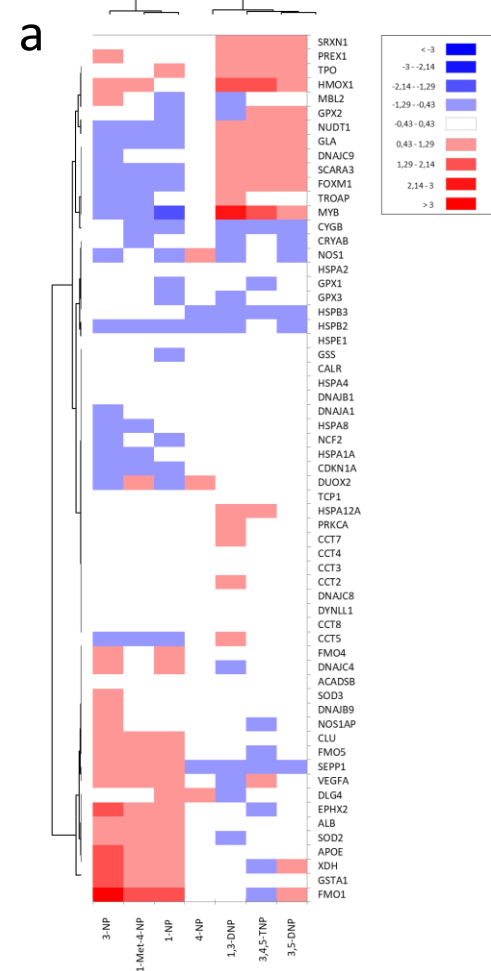
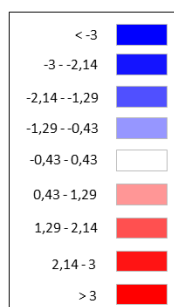
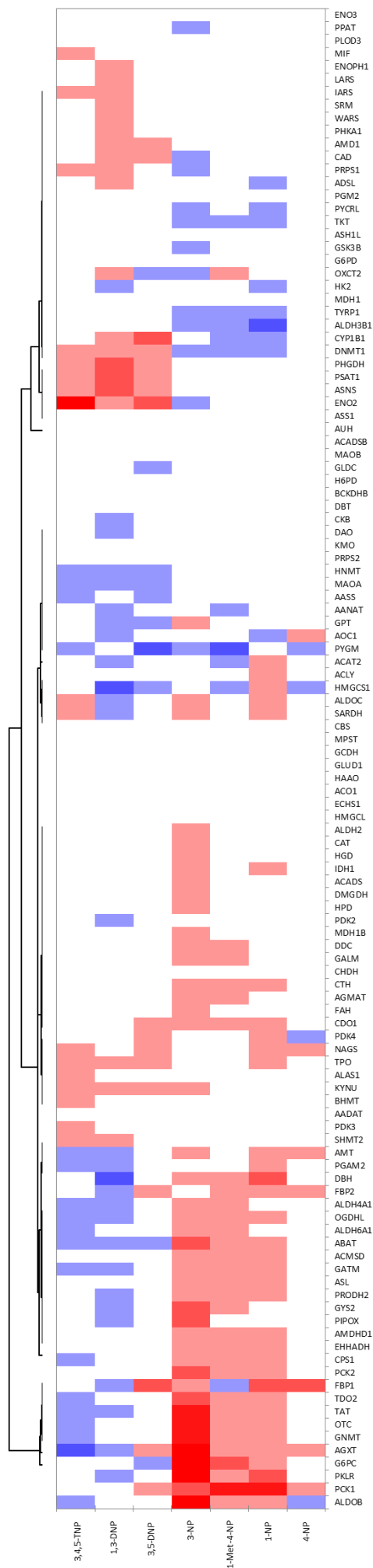
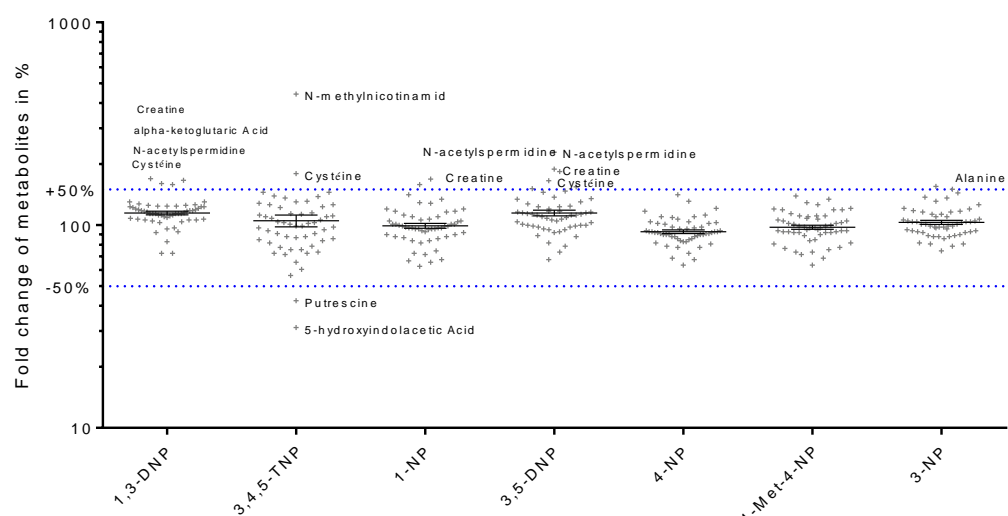


Figure 2

a



b



Molecules studied : alpha-ketoglutaric Acid, Acetylcholine, Aconitic Acid, Aspartic Acid, Citric Acid, Fumaric Acid, Glutamic Acid, Isocitric Acid, Malic Acid, N-acetylneuraminic Acid, Pantothenic Acid, Pyroglutamic Acid, Succinic Acid, 2-Methyl Hipuric Acid, 2-oxoglutaric Acid, 4-coumaric Acid, 5-hydroxyindolacetic Acid, Adenosine, Alanine, Arginine, Asparagine, Biotine, Choline, Choline phosphate, Creatine, Cystéine, Fructose-6-Phosphate, 3-Aminoisobutyric Acid, Glutamine, Reduced Glutathione, Glycero-3-phosphocholine, Histidine, Inosine, Isoleucine, Leucine, Lysine, Methionine, N-acetylornithine, N-acetylspermidine, NAD, Nicotinamide, N-methylnicotinamid, O-propanoylcarnitine, Ornithine, Phenylalanine, Proline, Putrescine, S-Adenosyl-L-Homocysteine, S-Adenosyl Methionine, Serine, Spermidine, Spermine, Threonine, Tyrosine, UDP-Glucose, and Valine.

Figure 3

Table 1. Overview of the different nitropyrazole-derived HEDMs used throughout this study

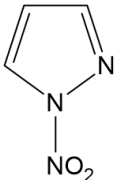
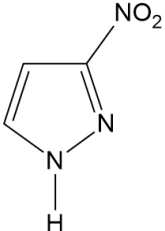
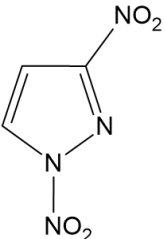
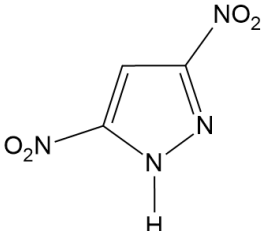
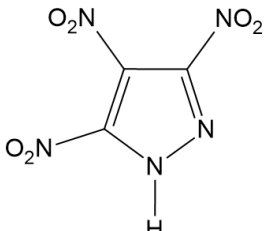
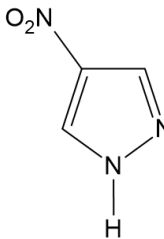
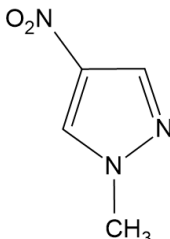
Name	1-Nitropyrazole (1-NP)	3-Nitropyrazole (3-NP)	1,3-Dinitropyrazole (1,3-DNP)	3,5-Dinitropyrazole (3,5-DNP)	3,4,5-Trinitropyrazole (3,4,5-TNP)	4-Nitropyrazole (4-NP)	1Methyl 4-Nitropyrazole (1-Met-4-NP)
Solvent	ACN	DMSO	Water	ACN	Water	ACN	ACN
Initial concentration	1 M	1 M	100 mM	770 mM	1 M	1 M	1 M
Structure							
Molecular weight (g/mol)	113.07	113.07	158.07	158.07	203.00	113.07	127.1

Table 2a. Cellular cytotoxicity of various concentrations of nitropyrazole-derived HEDMs measured using either an MTT assay (cell viability) or the xCELLigence technology (cell proliferation).

	BALB/3T3 clone (A31)	L5178Y TK +/- clone (3.7.2C)	CHO-K1			
	MTT IC ₅₀	MTT IC ₅₀	MTT IC ₅₀	x-CELLigence		
Molecules (vehicle)	mM	mM	mM	mM	% of confluence of treated condition (compared to the confluence of the control)	<i>P-value</i>
1-NP (ACN 0.1 %)	0.945 ± 0.154	1.690 ± 0.370	0.313 ± 0.090	1.000	97% ± 9%	NS
3-NP (DMSO 0.1 %)	1.230 ± 0.260	> 10	3.570 ± 0.850	1.250	35% ± 7%	*
				0.625	107% ± 10%	NS
1,3-DNP (water)	0.007 ± 0.003	0.006 ± 0.001	0.002 ± 0.001	0.007	7% ± 8%	**
				0.004	64% ± 15%	NS
				0.001	100% ± 20%	NS
3,5-DNP (ACN 0.1 %)	1.020 ± 0.430	1.100 ± 0.830	0.886 ± 0.015	1.020	52% ± 17%	NS
				0.500	97% ± 27%	NS
3,4,5-TNP (water)	0.038 ± 0.007	0.010 ± 0.001	0.034 ± 0.002	0.038	57% ± 3%	NS
				0.019	93% ± 33%	NS
4-NP (ACN 0.1 %)	3.000 ± 0.530	> 10	3.350 ± 0.860	10.000	8% ± 0%	*
				5.000	34% ± 5%	NS
				2.500	62% ± 8%	NS
				1.250	86% ± 19%	NS
				0.625	100% ± 2%	NS
1-Met-4-NP (ACN 0.1 %)	8.050 ± 0.750	> 10	> 10	10.000	28% ± 1%	NS
				5.000	65% ± 2%	NS
				2.500	68% ± 7%	NS
				1.250	115% ± 30%	NS

Table 2b. Cellular cytotoxicity of various concentrations of nitropyrazole-derived HEDMs measured using either an MTT assay (cell viability) or the xCELLigence technology (cell proliferation).					
	Human Fibroblast CRC05	Human Fibroblast PFS 04062			
	MTT IC ₅₀	MTT IC ₅₀	x-CELLigence		
Molecules (vehicle)	mM	mM	mM	% of confluence of treated condition (compared to the confluence of the control)	<i>P-value</i>
1-NP (ACN 0.1 %)	3.500	5.000 ± 0.770	5.7	84% ± 4%	NS
3-NP (DMSO 0.1 %)	> 10	> 10	10	30% ± 8%	*
			5	86% ± 25%	NS
			2.5	92% ± 16%	NS
			1.25	124% ± 0%	NS
1,3-DNP (water)	0.014	0.028 ± 0.006	0.019	0% ± 1%	**
			0.009	11% ± 3%	**
			0.004	55% ± 2%	NS
			0.002	105% ± 25%	NS
3,5-DNP (ACN 0.1 %)	> 10	6.250 ± 1.250	10.000	0% ± 4%	**
			5.000	8% ± 2%	**
			2.500	77% ± 2%	NS
			1.250	99% ± 0%	NS
3,4,5-TNP (water)	0.2	0.250 ± 0.020	0.250	2% ± 2%	**
			0.125	72% ± 7%	NS
			0.065	96% ± 11%	NS
			0.035	94% ± 21%	NS
4-NP (ACN 0.1 %)	ND	>10	5.000	47% ± 16%	NS
			2.500	49% ± 4%	NS
			1.250	59% ± 3%	NS
			0.625	78% ± 6%	NS
1-Met-4-NP (ACN 0.1 %)	ND	>10	5.000	70% ± 7%	NS
			2.500	78% ± 12%	NS
			1.250	72% ± 8%	NS
			0.625	106% ± 17%	NS

IC₅₀ : the concentration for which only there is 50 % of viable cells compared to the non-treated conditions at 72H. ND: not determined

Table 3a. Cytotoxic effects of various concentrations of nitropyrazole-derived HEDMs on proliferative and differentiated HepaRG cells.							
n=3-4	1-NP (ACN)	3-NP (DMSO)	1,3-DNP (water)	3,5-DNP (ACN)	3,4,5-TNP (water)	4-NP (ACN)	1-Met-4-NP (ACN)
Proliferative cells	0.850 ± 0.250 mM	> 10 mM	0.014 ± 0.003 mM	1.560 ± 0.510 mM	0.264 ± 0.040 mM	> 10 mM	> 10 mM
Differentiated cells	> 10 mM	8.300 ± 1.030 mM	0.105 ± 0.001 mM	5.700 ± 0.190 mM	0.205 ± 0.020 mM	> 10 mM	> 10 mM

Table 3b. Effect of the nitropyrazole-derived HEDMs on the cell cycle of proliferative HepaRG cells, measured via a flow cytometry analysis of BrdU incorporation into cells over 24 h							
	Concentration	S %	P-value	G2M %	P-value	G1 %	P-value
Water		18.4 ± 0.0		7.1 ± 0.0		71.5 ± 0.0	
1,3-DNP	0.05 mM	22.9 ± 1.5	*	11.7 ± 0.0	**	60.3 ± 0.3	****
3,4,5-TNP	0.25 mM	27.9 ± 1.2	****	11.8 ± 0.2	***	55.1 ± 1.3	****
DMSO 0.1%		14.7 ± 1.6		6.0 ± 0.1		75.9 ± 1.8	
3-NP	1.00 mM	15.9 ± 0.9	NS	8.4 ± 1.5	NS	71.5 ± 1.5	NS
ACN 0.1%		17.1 ± 1.1		5.6 ± 0.5		74.8 ± 0.7	
1-NP	1.00 mM	6.8 ± 0.9	****	8.6 ± 0.2	NS	77.2 ± 0.9	NS
3,5-DNP	1.00 mM	23.4 ± 0.8	**	8.7 ± 1.9	*	63.4 ± 2.3	****
4-NP	1.00 mM	15.4 ± 1.0	NS	7.6 ± 1.4	NS	73.8 ± 1.6	NS
1-Met-4-NP	1.00 mM	14.5 ± 0.4	NS	10.0 ± 0.3	**	72.6 ± 0.5	NS

Each condition was in duplicate, and at least three independent experiments were carried out.

Table 4. Variation in the expression of transcripts involved in cell death mechanisms in differentiated HepaRG cells treated for 24 h with nitropyrazole-derived HEDMs								
	Unchanged transcriptomics expression level of these genes	Gene variation (log2FdC)						
		3,4,5-TNP	1,3-DNP	3,5-DNP	3-NP	1-Met-4-NP	1-NP	4-NP
NECROSIS	ATP6V1G2, BMF, C1orf159, CCDC103, COMMD4, CYLD, DEFB1, DENND4A, DPYSL4, EIF5B, GALNT5, GRB2, HSPBAP1, PARP2, PVR, SPATA2, TMEM57, TXNL4B		PARP2 (↑)				GALTN5 (↓)	
AUTOPHAGY	AMBRA1, APP, ATG10, ATG12, ATG16L1, ATG16L2, ATG3, ATG4A, ATG4B, ATG4C, ATG4D, ATG5, ATG7, ATG9A, CLN3, CTSB, CXCR4, DRAM1, GABARAP, GABARAPL1, GABARAPL2, HDAC6, HSP90AA1, IGF1, LAMP1, MAP1LC3B, NPC1, PIK3R4, RAB24, RGS19, TMEM74, ULK1, UVRAG, WIP1		CXCR4 (↓) TMEM74 (↑)			CXCR4 (↑) IGF1 (↑)	CXCR4 (↑) IGF1 (↑)	IGF1 (↓)
SENESCENCE	BMI1, CD44, CDKN2C, CDKN2D, CITED2, COL1A1, COL3A1, CREG1, E2F3, EGR1, ETS1, ETS2, FN1, GLB1, HRAS, ID1, IGFBP3, IGFBP5, IGFBP7, ING1, IRF3, IRF5, IRF7, MAP2K1, MAP2K3, MAP2K6, MAPK14, MORC3, NOX4, PLAU, PRKCD, SERPINE1, SPARC, TERF2, TGFB1I1, THBS1, TWIST1, VIM	COL3A1 (↓) IGFBP3 (↑) SERPINE1 (↑)	IGFBP5 (↓) SERPINE1 (↑) TGFB1I1 (↓)	IGFBP5 (↓) SERPINE1 (↑)	SPARC (↑)	NOX4 (↑) PLAU (↓) VIM (↓)	COL1A1 (↑) IRF7 (↑) NOX4 (↑) VIM (↓)	

The increase with at least 50% is represented by (↑)

The decrease with at least 50% is represented by (↓)

24H exposure of differentiated Hepa-RG Cells

Exposure to no toxic concentrations of pyrazol

The fold changes are calculated with the vehicles control treated under the same experimental conditions

It is presented the mean of 3 independent experiments

Table 5. Proportion of apoptotic cells (early and late stage apoptosis) following the incubation of differentiated HepaRG cells with nitropyrazole-derived HEDMs for 24 h and 72 h.

	24 H								72 H							
Treatment	Dead cells	<i>p-value</i>	Late apoptotics cells	<i>p-value</i>	Early apoptotics cells	<i>p-value</i>	Live cells	<i>p-value</i>	Dead cells	<i>p-value</i>	Late apoptotics cells	<i>p-value</i>	Early apoptotics cells	<i>p-value</i>	Live cells	<i>p-value</i>
Water	6.49 ± 0.16		2.30 ± 0.17		0.91 ± 0.10		90.60 ± 0.50		8.40 ± 1.70		1.09 ± 0.89		0.23 ± 0.13		90.35 ± 2.65	
1,3-DNP 0.05 mM	6.60 ± 0.17	NS	1.45 ± 0.05	NS	0.43 ± 0.04	NS	91.70 ± 0.10	NS	9.76 ± 2.14	NS	0.94 ± 0.19	NS	0.18 ± 0.04	NS	89.25 ± 2.25	NS
3,4,5-TNP 0.25 mM	5.60 ± 0.19	NS	1.23 ± 0.26	NS	0.26 ± 0.10	NS	93.05 ± 0.25	NS	11.05 ± 0.05	NS	1.66 ± 0.12	NS	0.19 ± 0.01	NS	87.30 ± 0.10	NS
DMSO 0.1 %	6.62 ± 0.26		2.23 ± 0.10		0.91 ± 0.02		90.55 ± 0.45		10.63 ± 0.97		1.52 ± 0.01		0.24 ± 0.15		87.85 ± 0.85	
3-NP 1 mM	6.89 ± 1.06	NS	2.15 ± 0.23	NS	0.80 ± 0.17	NS	90.50 ± 1.50	NS	10.23 ± 0.47	NS	1.67 ± 0.12	NS	0.23 ± 0.01	NS	88.05 ± 0.65	NS
ACN 0.1 %	5.92 ± 0.12		1.69 ± 0.02		0.61 ± 0.04		92.05 ± 0.15		10.49 ± 1.02		1.44 ± 0.32		0.20 ± 0.06		88.00 ± 0.70	
1-NP 1 mM	7.65 ± 0.28	*	1.44 ± 0.28	NS	0.51 ± 0.02	NS	90.70 ± 0.60	NS	11.00 ± 0.30	NS	2.07 ± 0.04	NS	0.31 ± 0.01	NS	86.90 ± 0.30	NS
3,5-DNP 1mM	5.47 ± 0.24	NS	1.86 ± 0.02	NS	0.70 ± 0.01	NS	92.25 ± 0.15	NS	13.15 ± 0.25	NS	2.69 ± 0.65	NS	0.31 ± 0.06	NS	84.05 ± 0.95	*
4-NP 1mM	6.09 ± 0.15	NS	1.32 ± 0.45	NS	0.51 ± 0.08	NS	92.30 ± 0.30		11.50 ± 0.40	NS	1.37 ± 0.02	NS	0.31 ± 0.06	NS	87.10 ± 0.40	NS
1-Met-4-NP 1mM	5.58 ± 0.04	NS	1.50 ± 0.18	NS	0.28 ± 0.04	NS	92.80 ± 0.20	NS	9.64 ± 0.66	NS	1.54 ± 0.09	NS	0.37 ± 0.08	NS	88.60 ± 0.60	NS